CDT-RiskNet: A Risk-Aware Copula-Diffusion-Transformer Network for Stochastic EV Charging Station Optimization in Energy Market

Xihao Wang, *Graduate Student Member, IEEE*, Xiaojun Wang, *Member, IEEE*, Zhao Liu, *Member, IEEE*, Jianzhong Wu, *Fellow, IEEE*, Jinghan He, *Fellow, IEEE*,

***Abstract*—The growing penetration of photovoltaic (PV) systems and electric vehicles (EVs) poses systemic uncertainty for EV charging stations (EVCSs) participating in day-ahead energy market. These uncertainties are characterized by complex dependencies and time-varying tail risks that challenge traditional scenario generation and risk management techniques. This paper presents CDT-RiskNet, a Copula-Diffusion-Transformer framework for risk-aware stochastic optimization. A copula-enhanced diffusion model is developed to generate realistic joint scenarios of PV generation and EV charging demand. To manage time-varying tail risk, a Transformer-based risk module predicts dynamic CVaR weights from both historical and forecasted features, enabling coordinated evaluation across time. Simulation resultson both small-scale and large-scale EVCSs using real-world data demonstrate that CDT-RiskNet improves scenario generation quality, risk control, and adaptability to varying market conditions, leading to better economic performance under uncertainty.**

***Index Terms*—EV charging station, joint scenario generation, time-varying risk management, day-ahead energy market.**

I. Introduction

THE decarbonization of power and transportation sectors has become a global priority, hence the growing interest in electric vehicles (EVs) and photovoltaic (PV) systems [1]. According to the International Energy Agency (IEA), global EV sales surpassed 17 million units in 2024, representing nearly 20% of new car sales, and are projected to reach more than 40% by 2030 under current policy scenarios [2]. By integrating on-site PV, energy storage systems (ESSs), and vehicle-to-grid (V2G) technologies, urban EV charging stations (EVCSs) can actively participate in the energy market to optimize energy procurement, provide grid services, and enhance cost-effectiveness and operational sustainability [3].

However, the uncertainties of PV generation and EV charging demand exhibit nonlinear and time-varying statistical dependence due to shared exogenous drivers and temporal characteristics [4], which critically impact EVCS decision-making in energy markets. The source-load uncertainty introduces two key challenges. First, their externally driven statistical dependence implies that independently modeling PV generation and EV charging demand may distort their joint statistical structure and lead to unrealistic operating scenarios, thereby necessitating accurate joint scenario generation [5]. Second, the temporal variability of uncertainty and interdependence motivate the need for time-varying risk management [6].

Scenario generation plays a crucial role in characterizing uncertainty for robust decision-making [7]. Statistical methods, such as Monte Carlo Simulation (MCS) [8] and Gaussian Mixture Models (GMMs) [9], rely heavily on prior probability distributions, which limits their ability to capture complex and dynamic uncertainty patterns. Moreover, these methods alone often fail to capture the dependence between PV generation and EV charging demand, limiting their effectiveness in modeling real-world uncertainties. Some methods, such as Copula-based modeling, explicitly capture dependence structures and have been employed to improve source-load correlation modeling. Carmona et al. leveraged copula-based modeling to capture the joint behavior of load, solar, and wind power, enabling the generation of correlated multivariate scenarios [10]. However, such methods still rely on parametric and distribution assumptions, which constrain their ability to adapt to nonstationary, high-dimensional uncertainty. In contrast, data-driven approaches have gained attention for their ability to learn patterns directly from historical data without rigid prior assumptions [11]. Deep generative models, including Variational Autoencoders (VAEs) [12] and Generative Adversarial Networks (GANs) [13], [14], have been applied to scenario generation, showing promising results in capturing marginal distributions. Recently, Diffusion Models have emerged as a powerful alternative, capable of learning complex, multi-modal distributions [15], [16], [17], [18]. While most existing diffusion-based methods have focused on modeling individual variables, limited attention has been given to preserving the joint dependence structures inherent in source-load interactions. Zhao et al. proposed a conditional diffusion-based scenario generation model that captures the spatiotemporal correlations between source and load, enabling the generation of joint scenarios [19]. Although the accuracy of joint scenario generation has improved in these studies, there is still a time-varying tail risk that cannot be addressed by scenario realism alone [20]. To solve this, it is necessary to develop a dynamic risk management mechanism that can capture the characteristics of risk varying over time.

The dynamic tail risk often becomes more severe during periods of high volatility of PV generation or of inflexible EV charging demand. Conditional Value at Risk (CVaR) is widely used in stochastic optimization to manage tail risks [21], [22], [23], [24]. CVaR-based methods have been applied to energy market optimization, such as multi-temporal bidding strategies for virtual power plants under renewable and market uncertain-

This work was supported by the National Nature Science Foundation of China under Grant U24B208. *(Corresponding author: Xiaojun Wang)*

Xihao Wang, Xiaojun Wang, Zhao Liu, and Jinghan He are with the School of Electrical Engineering, Beijing Jiaotong University, Beijing 100044, China (email:xihao_wang@bjtu.edu.cn; xjwang1@bjtu.edu.cn; liuzhao1@bjtu.edu.cn; jhhe@bjtu.edu.cn)

Jianzhong Wu is with the School of Engineering, Cardiff University, Cardiff CF24 3AA, U.K. (email: wuj5@cardiff.ac.uk)

TABLE I
LITERATURE REVIEW

Reference	Scenario Generation			Risk Management	
	Statistical	Data-Driven	Dependence Modeling	Static CVaR	TW-CVaR
[8] - [9]	√				
[10]	√		√		
[11]- [18]		√			
[19]		√	√		
[21]	√			√	
[22]- [26]				√	
[27]					√
Proposed		√	√		√

ties [25], and retailer-side models incorporating flexible EV participation and temporal demand characteristics [26]. These CVaR-based approaches have shown effectiveness in balancing expected return and extreme risks. However, to better reflect the temporal dynamics of uncertainty and risk, several studies have further explored time-varying CVaR formulations, which allow the risk preference to adapt across different time periods. Vardanyan et al. introduced hourly CVaR constraints in hydropower bidding to independently control risk at each time slot [27]. In the context of day-ahead market participation, EVCS operators must assess risk and performance over the entire operational horizon [28]. A unified CVaR formulation with time-varying risk weights allows for coordinated risk evaluation across all time periods, and achieves more balanced resource scheduling. To generate time-varying CVaR weights, one intuitive approach is to extract empirical distributions from historical records corresponding to the same time periods. But this method lacks the ability to anticipate shifts in future scenario characteristics. A more adaptive strategy first searches optimal weight vectors by solving CVaR-based optimization problems on historical samples, and then trains sequence models such as Long Short-Term Memory Network (LSTM) to learn the mapping from uncertainty patterns to risk weights. However, LSTM is limited in capturing long-range dependencies. Transformer networks offer a more flexible alternative by leveraging attention mechanisms [29], which allow the model to focus on relevant patterns across historical and forecasted scenario features, enabling more accurate learning of time-varying risk weights. Table I summarizes representative studies on scenario generation and risk management, highlighting the need for a unified framework that jointly integrates scenario generation and dynamic risk modeling to address time-varying source-load uncertainty.

This study proposes CDT-RiskNet, a unified Copula–Diffusion–Transformer framework for risk-aware stochastic optimization. Unlike single diffusion or other generative models that ignore source–load dependencies, CDT-RiskNet embeds a dynamic copula into the diffusion process to preserve nonlinear and time-varying PV–EV interactions. Compared with CVaR approaches with static risk weights, the proposed Transformer-based mechanism learns time-varying CVaR weights directly from historical and forecasted features, thereby capturing the temporal dynamics of risk. This unified design not only enhances the fidelity and diversity of joint scenarios but also enables adaptive risk management across the entire operational horizon, resulting in more robust and cost-effective EVCS market participation under complex uncertainties. The contributions of this study are as follows:

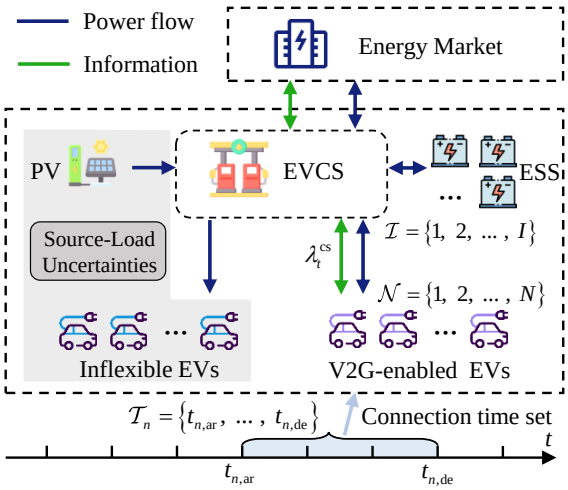

Fig. 1. The structure of the EVCS operation in energy market.

1) A copula-diffusion model is developed to explicitly preserve the nonlinear and time-varying dependencies between PV generation and EV charging demand during scenario generation, thereby overcoming the limitations of conventional diffusion models that focus only on marginal distributions, and producing joint scenarios that are both dependence-faithful and sufficiently diverse.
2) A time-varying CVaR formulation is introduced in which dynamic risk weights are learned through a Transformer from historical and forecast features, enabling temporally adaptive risk control beyond static-weight CVaR.
3) The CDT-RiskNet is established to integrate scenario generation and risk-aware optimization into a unified framework, achieving improved economic performance in EVCS market operations under complex uncertainties, while maintaining robust performance under varying market conditions and weather fluctuations.

While this study focuses on the EVCS case, CDT-RiskNet framework is generally applicable to stochastic optimization under joint uncertainties in power systems. The rest of this paper is organized as follows. Section II formulates the stochastic optimization and time-varying risk management model. Section III details the proposed CDT-RiskNet framework. Section IV presents numerical studies. Section V concludes the paper.

II. Problem Formulation

This section presents the operational model of the EVCS, followed by the stochastic optimization framework and the time-varying risk management formulation. The key challenges addressed in this study are also highlighted.

Fig. 1 illustrates the structure of the EVCS, which consists of inflexible EVs, V2G-enabled EVs, an on-site PV system, and an ESS. The EVCS procures electricity from the market and supplements it with locally generated PV power. By coordinating the charging and discharging of V2G-enabled EVs and ESS, the EVCS engages in energy market while ensuring that all EVs meet their required charging demands. A bilevel

stochastic optimization framework models the interaction between the EVCS and V2G-enabled EVs. In the upper level, the EVCS sets electricity prices λ_t^{cs} based on market signals to guide the charging and discharging behaviors of V2G-enabled EVs, aiming to maximize its own profit. At the lower level, each V2G-enabled EV optimizes its charging schedule in response to the price to minimize its cost. Within this framework, uncertainties arise from stochastic PV generation and the charging demands of inflexible EVs.

The EVCS participates in the day-ahead energy market. The operating horizon is divided into T discrete time periods, indexed by $t \in \{1, 2, ..., T\}$. Let $\mathcal{N} = \{1, 2, ..., N\}$ denote the set of V2G-enabled EVs, and let $\mathcal{I} = \{1, 2, ..., I\}$ represent the set of batteries in the ESS. The arrival and departure times of the V2G-enabled EV n are denoted as $t_{n,\text{ar}}$ and $t_{n,\text{de}}$, and its connection time set is given by $\mathcal{T}_n = \{t_{n,\text{ar}}, ..., t_{n,\text{de}}\}$.

A. Stochastic Optimization

The bilevel stochastic optimization problem is formulated using a scenario-based framework, considering the source-load uncertainties from PV generation and inflexible EV charging demands. Let $m \in \mathcal{M}$ denote the scenario index.

The upper-level objective function aims to maximize EVCS's profits from EV charging services and energy trading while accounting for ESS degradation cost. The EVCS is modeled as a price taker in the day-ahead energy market. This assumption is commonly adopted for EVCS when the focus is on uncertainty modeling and risk-aware scheduling [30].

$$\max_{\lambda_t^{\text{cs}}, \mathcal{B}_{i,t,m}^{+}, \mathcal{B}_{i,t,m}^{-}, \mathcal{P}_{t,m}^{\text{buy}}, \mathcal{P}_{t,m}^{\text{sell}}} \sum_{m \in \mathcal{M}} \pi_m \mathcal{F}_m^{\text{EVCS}} \tag{1a}$$

$$\mathcal{F}_m^{\text{EVCS}} = \mathcal{R}_m^{\text{serv}} + \mathcal{R}_m^{\text{em}} - \mathcal{C}_m^{\text{deg}} \tag{1b}$$

$$\mathcal{R}_m^{\text{serv}} = \sum_{t \in \mathcal{T}} \sum_{n \in \mathcal{N}} \lambda_t^{\text{cs}} \left(\eta^{\text{ch}} \left(\mathcal{P}_{n,t}^{+} + \mathcal{P}_{t,m}^{\text{IEV}} \right) - \frac{\mathcal{P}_{n,t}^{-}}{\eta^{\text{dis}}} \right) \Delta t \tag{1c}$$

$$\mathcal{R}_m^{\text{em}} = \sum_{t \in \mathcal{T}} \left(\lambda_t^{\text{sell}} \mathcal{P}_{t,m}^{\text{sell}} - \lambda_t^{\text{buy}} \mathcal{P}_{t,m}^{\text{buy}} \right) \Delta t \tag{1d}$$

$$\mathcal{C}_m^{\text{deg}} = \lambda^{\text{cell}} \sum_{t \in \mathcal{T}} \sum_{i \in \mathcal{I}} \left(\eta^{\text{ch}} \mathcal{B}_{i,t,m}^{+} + \frac{\mathcal{B}_{i,t,m}^{-}}{\eta^{\text{dis}}} \right) \Delta t \tag{1e}$$

where $\mathcal{B}_{i,t,m}^{+}$ and $\mathcal{B}_{i,t,m}^{-}$ are the charging/discharging power of battery i in the ESS, while $\mathcal{P}_{t,m}^{\text{buy}}$ and $\mathcal{P}_{t,m}^{\text{sell}}$ are market purchase and sale powers. π_m is the probability of scenario m. $\mathcal{R}_m^{\text{serv}}$ is EV charging profit, considering efficiency $\left(\eta^{\text{ch}}, \eta^{\text{dis}}\right)$, EV power $\left(\mathcal{P}_{n,t}^{+}, \mathcal{P}_{n,t}^{-}\right)$, and inflexible EV charging demand $\mathcal{P}_{t,m}^{\text{IEV}}$. A symmetric price λ_t^{cs} is assumed between EVs and the EVCS, following common practice in EVCS scheduling [31]. $\mathcal{R}_m^{\text{em}}$ is energy market profit from selling at price λ_t^{sell} and buying at λ_t^{buy}. $\mathcal{C}_m^{\text{deg}}$ is the degradation cost of the ESS, the linear form is an acceptable approximation for day-ahead operation, consistent with common practice [32]. λ^{cell} is the unit degradation cost. Δt is the duration of time step.

The constraints describe the operational characteristics and decision-making rules of the EVCS.

$$\mathcal{P}_{t,m}^{\text{PV}} + \mathcal{P}_{t,m}^{\text{buy}} + \sum_{i \in \mathcal{I}} \mathcal{B}_{i,t,m}^{-} + \sum_{n \in \mathcal{N}} \mathcal{P}_{n,t}^{-} = \mathcal{P}_{t,m}^{\text{sell}} + \sum_{i \in \mathcal{I}} \mathcal{B}_{i,t,m}^{+} + \sum_{n \in \mathcal{N}} \mathcal{P}_{n,t}^{+} + \mathcal{P}_{t,m}^{\text{IEV}}, \quad \forall m \in \mathcal{M}, \forall t \in \mathcal{T} \tag{2a}$$

$$0 \le \mathcal{P}_{t,m}^{\mathcal{A}} \le \bar{\mathcal{P}}_t^{\mathcal{A}} z_{t,m}^{\mathcal{A}}, \quad \forall t \in \mathcal{T}, \forall m \in \mathcal{M}, \mathcal{A} \in \{\text{buy}, \text{sell}\} \tag{2b}$$

$$\sum_{\mathcal{A} \in \{\text{buy,sell}\}} z_{t,m}^{\mathcal{A}} \le 1, \quad \forall t \in \mathcal{T}, \forall m \in \mathcal{M} \tag{2c}$$

$$S_{i,t+1,m} = S_{i,t,m} + \left(\eta^{\text{ch}} \mathcal{B}_{i,t,m}^{+} - \frac{\mathcal{B}_{i,t,m}^{-}}{\eta^{\text{dis}}} \right) \frac{\Delta t}{\mathcal{E}_i^{\text{bat}}}, \quad \forall i \in \mathcal{I}, \forall t \in \mathcal{T}, \forall m \in \mathcal{M} \tag{2d}$$

$$\underline{S}_i \le S_{i,t,m} \le \overline{S}_i, \quad \forall i \in \mathcal{I}, \forall t \in \mathcal{T}, \forall m \in \mathcal{M} \tag{2e}$$

$$0 \le \mathcal{B}_{i,t,m}^{\mathcal{X}} \le \bar{\mathcal{B}}_i^{\mathcal{X}} z_{i,t,m}^{\mathcal{X}}, \quad \forall i \in \mathcal{I}, \forall t \in \mathcal{T}, \forall m \in \mathcal{M}, \mathcal{X} \in \{+, -\} \tag{2f}$$

$$\sum_{\mathcal{X} \in \{+,-\}} z_{t,m}^{\mathcal{X}} \le 1, \quad \forall t \in \mathcal{T}, \forall m \in \mathcal{M}, \mathcal{X} \in \{+, -\} \tag{2g}$$

$$\frac{1}{|\mathcal{T}|} \sum_{t \in \mathcal{T}} \lambda_t^{\text{cs}} = \mu \tag{2h}$$

$$\underline{\lambda}^{\text{cs}} \le \lambda_t^{\text{cs}} \le \overline{\lambda}^{\text{cs}}, \quad \forall t \in \mathcal{T} \tag{2i}$$

Power balance (2a) ensures that total power supply, including PV generation $\mathcal{P}_{t,m}^{\text{PV}}$, $\mathcal{P}_{t,m}^{\text{buy}}$, $\mathcal{B}_{i,t,m}^{-}$, and $\mathcal{P}_{n,t}^{-}$, matches total power demand, including $\mathcal{P}_{t,m}^{\text{sell}}$, $\mathcal{B}_{i,t,m}^{+}$, $\mathcal{P}_{n,t}^{+}$, and $\mathcal{P}_{t,m}^{\text{IEV}}$. Market limits (2b) and (2c) constrain transaction power $\mathcal{P}_{t,m}^{\mathcal{A}}$ ($\mathcal{A} \in \{\text{buy}, \text{sell}\}$) with bounds $\bar{\mathcal{P}}_t^{\mathcal{A}}$ and binary variables $z_{t,m}^{\mathcal{A}}$ preventing simultaneous transactions. ESS dynamics (2d) and (2e) update the state-of-charge (SOC) $S_{i,t,m}$, and enforce limits $\left[\underline{S}_i, \overline{S}_i\right]$. $\mathcal{E}_i^{\text{bat}}$ is the battery capacity. (2f) and (2g) limit ESS power $\mathcal{B}_{i,t,m}^{\mathcal{X}}$ ($\mathcal{X} \in \{+, -\}$) with binary variables that ensure no simultaneous operations. Pricing constraints (2h) and (2i) enforce λ_t^{cs} to align with the average price μ and to remain within $\left[\underline{\lambda}^{\text{cs}}, \overline{\lambda}^{\text{cs}}\right]$.

The objective of the lower-level EV model aims to minimize charging cost and battery degradation cost.

$$\min_{\mathcal{P}_{n,t}^{+}, \mathcal{P}_{n,t}^{-}} \sum_{t \in \mathcal{T}_n} \lambda_t^{\text{cs}} \left(\mathcal{P}_{n,t}^{+} - \mathcal{P}_{n,t}^{-} \right) \Delta t + \lambda^{\text{cell}} \sum_{t \in \mathcal{T}_{n,a}} \left(\eta^{\text{ch}} \mathcal{P}_{n,t}^{+} + \frac{\mathcal{P}_{n,t}^{-}}{\eta^{\text{dis}}} \right) \Delta t \tag{3}$$

For the V2G-enabled EVs, the operational constraints are as follows.

$$0 \le \mathcal{P}_{n,t}^{\mathcal{X}} \le \bar{\mathcal{P}}_n z_{n,t}^{\mathcal{X}}, \quad \forall n \in \mathcal{N}, \forall t \in \mathcal{T}_n, \mathcal{X} \in \{+, -\} \tag{4a}$$

$$\sum_{\mathcal{X} \in \{+,-\}} z_{n,t}^{\mathcal{X}} \le 1, \quad \forall n \in \mathcal{N}, \forall t \in \mathcal{T}_n, \mathcal{X} \in \{+, -\} \tag{4b}$$

$$\mathcal{P}_{n,t}^{+} = \mathcal{P}_{n,t}^{-} = 0, \quad z_{n,t}^{+} = z_{n,t}^{-} = 0, \quad \forall n \in \mathcal{N}, \forall t \notin \mathcal{T}_n \tag{4c}$$

$$S_{n,t+1} = S_{n,t} + \left(\eta^{\text{ch}} \mathcal{P}_{n,t}^{+} - \frac{\mathcal{P}_{n,t}^{-}}{\eta^{\text{dis}}} \right) \frac{\Delta t}{\mathcal{E}_n}, \quad \forall n \in \mathcal{N}, \forall t \in \mathcal{T}_n \tag{4d}$$

$$\underline{S}_n \le S_{n,t} \le \overline{S}_n, \quad \forall n \in \mathcal{N}, \forall t \in \mathcal{T}_n \tag{4e}$$

$$S_{n,t_{de}} \ge S_n^{\text{re}}, \quad \forall n \in \mathcal{N} \tag{4f}$$

The power limits (4a) restrict $\mathcal{P}_{n,t}^{+}$ and $\mathcal{P}_{n,t}^{-}$ to their bounds $\bar{\mathcal{P}}_n$, controlled by binary variables $z_{n,t}^{+}$ and $z_{n,t}^{-}$, preventing

simultaneous operation in (4b). When the EV is not connected to the charger ($t \notin \mathcal{T}_n$), all associated power and binary variables are set to zero in (4c). (4d) updates the SOC $S_{n,t}$ of EV n, where $\mathcal{E}_n$ is the EV battery capacity. The SOC remains within $\left[\underline{S}_n, \overline{S}_n\right]$ during the connection period in (4e), and meets the required level S_n^{re} at departure in (4f).

Based on the transformation methods in [31] and [33], the bilevel stochastic optimization model is transformed into a single-level problem using KKT conditions. An affine adjustment method used in [34] is then adopted to derive a unified decision policy. The recourse variables are expressed as affine functions of the realized uncertainty:

$$\begin{bmatrix} \mathcal{B}_{i,t,m}^{+} \\ \mathcal{B}_{i,t,m}^{-} \\ \mathcal{P}_{t,m}^{\text{buy}} \\ \mathcal{P}_{t,m}^{\text{sell}} \end{bmatrix} = \begin{bmatrix} \mathcal{B}_{i,t}^{+} \\ \mathcal{B}_{i,t}^{-} \\ \mathcal{P}_{t}^{\text{buy}} \\ \mathcal{P}_{t}^{\text{sell}} \end{bmatrix} + \begin{bmatrix} \phi_{i,t}^{+} \\ \phi_{i,t}^{-} \\ \phi_{t}^{b} \\ \phi_{t}^{s} \end{bmatrix} \cdot \vartheta_{t,m} \tag{5}$$

The scalar $\vartheta_{t,m}$ characterizes the realization of source-load uncertainty at time t under scenario m. The affine coefficients $\phi_{i,t}^{+}$, $\phi_{i,t}^{-}$, ϕ_t^b, and ϕ_t^s determine how each decision variable adjusts in response to uncertainty. To ensure that the total adjustment is properly distributed among different control actions, the affine coefficients satisfy:

$$\phi_{i,t}^{+} + \phi_{i,t}^{-} + \phi_t^b + \phi_t^s = 1 \tag{6}$$

The affine adjustment scheme allows real-time uncertainty to be absorbed through adaptive recourse decisions.

B. Time-Varying Risk Management

To manage uncertainties associated with PV generation and inflexible EV charging demands, this study proposes a risk management model based on CVaR formulated directly in terms of profit. The proposed CVaR measures the expected profits falling below a specified confidence level α, ensuring robustness against scenarios with extremely low profitability.

Traditional CVaR approaches assume a constant weight of risk across all time periods, failing to capture the time-varying nature of uncertainty and correlation. To address this limitation, this study introduces a time-varying weighted CVaR (TW-CVaR) formulation, allowing dynamic adjustments of risk assessment over the operating horizon. Let $\mathcal{L}_{t,m}$ denote the profit function under scenario m at time t. The TW-CVaR over the time horizon $\mathcal{T}$ is defined as:

$$\text{TW-CVaR}_\alpha = \max_{\nu_t} \left\{ \sum_{t \in \mathcal{T}} w_t \left(\nu_t - \frac{1}{1-\alpha} \sum_{m \in \mathcal{M}} \pi_m \max\left(\nu_t - \mathcal{L}_{t,m}, 0\right) \right) \right\} \tag{7}$$

where ν_t is the Value-at-Risk (VaR) at confidence level α, and w_t denotes the time-varying weights that reflect the relative importance of risk at each time step t. The weights w_t are normalized such that $\sum_{t \in \mathcal{T}} w_t = 1$, ensuring consistency in the risk assessment across the horizon.

Therefore, the upper-level objective function (1a) should be reformulated as:

$$\max (1-\psi) \sum_{m \in \mathcal{M}} \pi_m \mathcal{F}_m^{\text{EVCS}} + \psi(\text{TW-CVaR}_\alpha) \tag{8}$$

where ψ represents the risk aversion coefficient.

Remark (Challenges in stochastic optimization and risk management). The stochastic optimization model incorporates PV generation $\mathcal{P}_{t,m}^{\text{PV}}$ and inflexible EV charging demands $\mathcal{P}_{t,m}^{\text{IEV}}$ under scenario m in (2a), both of which exhibit high volatility and strong interdependence. Accurately modeling their joint uncertainty without restrictive prior assumptions remains a challenge. In time-varying risk management, the correlation and variability of PV generation and EV charging demand fluctuate over time, necessitating time-varying risk weighting via w_t. However, a key challenge lies in how to effectively leverage both historical and forecasted information to generate w_t that accurately maps underlying uncertainty patterns to appropriate risk levels.

These challenges underscore the need for a unified data-driven framework capable of generating realistic joint scenarios and dynamically adjusting risk weights based on temporal uncertainty patterns. CDT-RiskNet can provide these key inputs for stochastic optimization and time-varying risk management, ensuring adaptive decision-making under uncertainty.

III. Proposed CDT-RiskNet for Risk-Aware Stochastic Optimization

This section presents CDT-RiskNet as a unified framework for scenario generation and risk management, as outlined in Fig. 2. It consists of three key components: the Copula Layer captures source-load dependencies, providing conditional inputs for subsequent modules. The Diffusion Layer generates realistic joint scenarios. And the Transformer Layer models temporal risk variations to produce risk coefficients.

A. Forward Diffusion for Source-Load Historical Observations

Diffusion models have demonstrated strong generative capabilities by progressively adding noise to data during a forward diffusion process, then learning to reverse this process to generate new samples. In the proposed framework, the Diffusion Layer is employed to generate realistic joint scenarios for PV generation and inflexible EV charging demand.

Let the historical time series data of PV generation and inflexible EV charging demand be denoted as $\mathbf{x}_0^{\alpha}$ and $\mathbf{x}_0^{\beta}$, respectively. The joint source-load state at each time step is represented as a concatenated vector $\mathbf{x}_0 = \left(\mathbf{x}_0^{\alpha}, \mathbf{x}_0^{\beta}\right)$, where $\mathbf{x}_0 \in \mathbb{R}^{2T}$. The goal of scenario generation is to obtain a set of M diverse realistic joint realizations, denoted as: $\mathbb{S} = \left\{\mathbf{x}_0^{(1)}, \mathbf{x}_0^{(2)}, \ldots, \mathbf{x}_0^{(M)}\right\}$, where each sample $\mathbf{x}_0^{(m)} \sim q(\mathbf{x}_0)$ represents a possible realization of the joint PV-EV uncertainty over the time horizon T. Additionally, let $\mathbf{e}_t$ represent external factors, including weather data and calendar data.

To generate $\mathbb{S}$, the diffusion process progressively perturbs the original data $\mathbf{x}_0$ over K steps by injecting Gaussian noise, yielding intermediate states $\mathbf{x}_k$. As $k \to K$, $\mathbf{x}_k$ approaches an isotropic Gaussian distribution $\mathcal{N}(0, I)$, serving as the

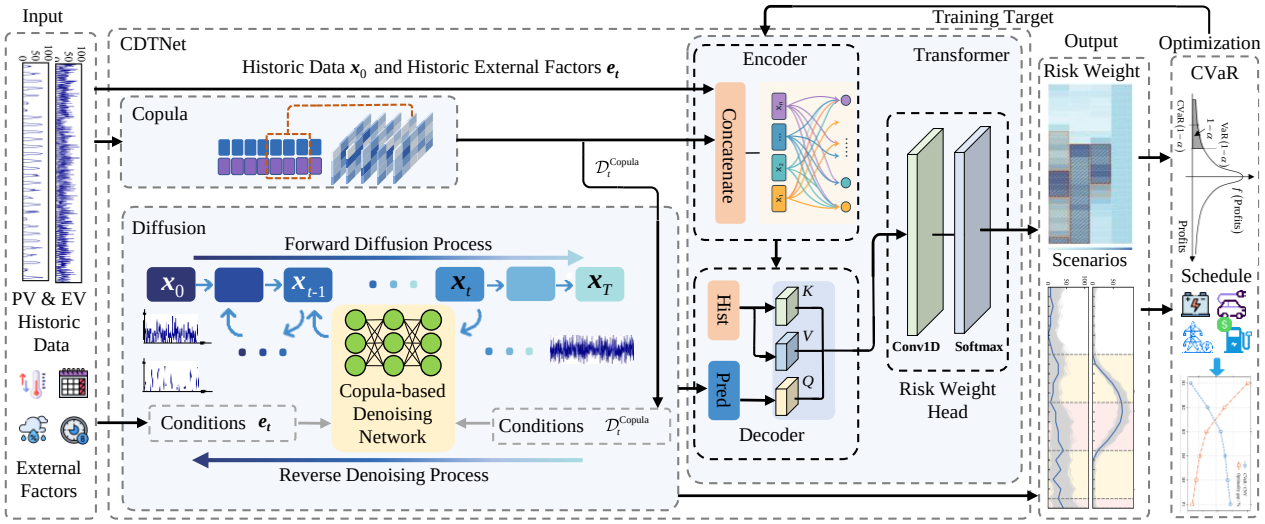

Fig. 2. The framework of CDT-RiskNet for risk-aware stochastic optimization of EVCS operations.

initialization for the reverse denoising process. The forward diffusion process follows a Markovian structure, defined as:

$$q(\mathbf{x}_{1:K} \mid \mathbf{x}_0) = \prod_{k=1}^{K} q(\mathbf{x}_k \mid \mathbf{x}_{k-1}) \tag{9}$$

where the transition distribution $q(\mathbf{x}_k \mid \mathbf{x}_{k-1})$ is defined as:

$$q(\mathbf{x}_k \mid \mathbf{x}_0) = \mathcal{N}\left(\mathbf{x}_k; \sqrt{\alpha_k}\mathbf{x}_0, (1-\alpha_k)\mathbf{I}\right) \tag{10}$$

where $\beta_k \in (0,1)$ is a noise schedule controlling the variance of the added noise, with $\alpha_k := 1 - \beta_k$, and cumulative decay factor $\bar{\alpha}_k := \prod_{i=1}^{k} \alpha_i$. Consequently, $\mathbf{x}_k$ can be expressed as:

$$\mathbf{x}_k = \sqrt{\bar{\alpha}_k}\mathbf{x}_0 + \sqrt{1-\bar{\alpha}_k}\boldsymbol{\epsilon}, \quad \boldsymbol{\epsilon} \sim \mathcal{N}(0, \mathbf{I}) \tag{11}$$

where $\boldsymbol{\epsilon}$ is sampled from a standard Gaussian distribution. The detailed proofs of (10) and (11) are provided in [15].

B. Reverse Denoising under Dynamic Copula-Based Correlation

To generate realistic joint time-series scenarios of PV generation and inflexible EV charging demands, the Diffusion Layer employs a structured reverse denoising process. This process iteratively removes noise from an initial Gaussian distribution, progressively recovering realistic joint samples. To capture the nonlinear and time-varying dependence between PV generation $\mathbf{x}_0^{\alpha}$ and inflexible EV charging demand $\mathbf{x}_0^{\beta}$, the reverse diffusion process is guided by conditional inputs from both external factors $\mathbf{e}_t$ and a dynamic Copula Layer. The dependence structure from the Copula Layer is represented by a time series of correlation coefficients $\mathcal{D}_t^{\text{Copula}}$.

The historical data are first mapped onto a standard normal space using a probability integral transform:

$$z^{\alpha} = \Phi^{-1}\left(F_{\alpha}(\mathbf{x}_0^{\alpha})\right), \quad z^{\beta} = \Phi^{-1}\left(F_{\beta}(\mathbf{x}_0^{\beta})\right) \tag{12}$$

where $F_{\alpha}(\cdot)$ and $F_{\beta}(\cdot)$ are the marginal cumulative distribution functions (CDFs) of PV generation and EV charging demand, and $\Phi^{-1}(\cdot)$ is the inverse standard normal CDF.

The dynamic dependence between the two processes is modeled by a time-varying correlation coefficient ρ_t, which evolves according to a constrained autoregressive moving average (ARMA)-type equation:

$$\rho_t = \tilde{\Lambda}\Big(\omega_\rho - \beta_\rho \rho_{t-1} + \alpha_\rho \frac{1}{L}\sum_{j=1}^{L} z_{t-j}^{\alpha} z_{t-j}^{\beta}\Big) \tag{13}$$

where L is the window length. ω_ρ, β_ρ and α_ρ are parameters estimated via maximum likelihood. $\tilde{\Lambda}(\cdot)$ is a modified logistic transformation $\tilde{\Lambda}(x) = \tanh(x/2)$ that ensures $\rho_t \in (-1, 1)$. The dynamic copula conditioning variable is given by:

$$\mathcal{D}_t^{\text{Copula}} = \rho_t, \tag{14}$$

Starting from an initial Gaussian sample $\mathbf{x}_K$, the reverse process is formulated as:

$$p_\theta(\mathbf{x}_{0:K}) = p(\mathbf{x}_K) \prod_{k=1}^{K} p_\theta(\mathbf{x}_{k-1} \mid \mathbf{x}_k, \mathbf{e}_t, \mathcal{D}_t^{\text{Copula}}) \tag{15}$$

where $p_\theta(\mathbf{x}_{k-1} \mid \mathbf{x}_k, \mathbf{e}_t, \mathcal{D}_t^{\text{Copula}})$ represents the transition probability from state $\mathbf{x}_k$ to state $\mathbf{x}_{k-1}$, conditioned on $\mathbf{e}_t$ and $\mathcal{D}_t^{\text{Copula}}$, and parameterized by θ. The conditioning variables $\mathbf{e}_t$ and $\mathcal{D}_t^{\text{Copula}}$ are fixed for each operational period t and shared across all diffusion steps.

$$p_\theta(\mathbf{x}_{k-1} \mid \mathbf{x}_k, \mathbf{e}_t, \mathcal{D}_t^{\text{Copula}}) = \mathcal{N}\left(\mathbf{x}_{k-1}; \mu_\theta(\mathbf{x}_k, k, \mathbf{e}_t, \mathcal{D}_t^{\text{Copula}}), \Sigma_k\right) \tag{16}$$

where $\mu_\theta(\mathbf{x}_k, k, \mathbf{e}_t, \mathcal{D}_t^{\text{Copula}})$ is the predicted mean incorporating dependence constraints, and the covariance matrix Σ_k captures stepwise uncertainty.

In the training phase, we adopt an objective derived from the evidence lower bound (ELBO) that minimizes the mean squared error (MSE) between the true noise and the noise predicted by the denoising network. For each historical joint observation $\mathbf{x}_0$ and a diffusion step k uniformly sampled from $\{1, ..., K\}$, a noisy sample $\mathbf{x}_k$ is generated according to (11),

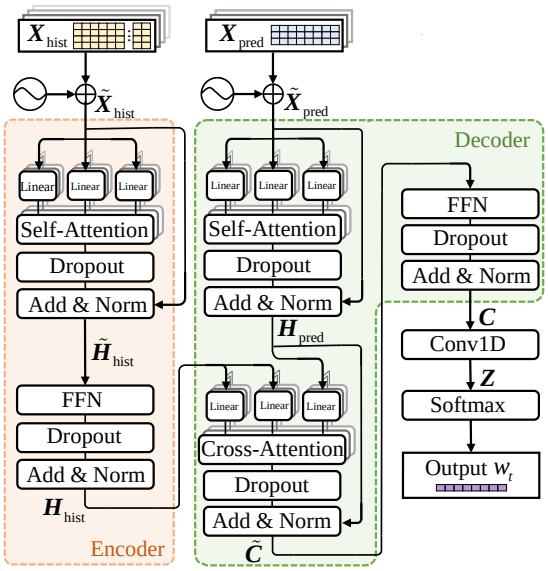

Fig. 3. The architecture of Transformer-based time-varying weighting.

where Gaussian noise $\boldsymbol{\epsilon} \sim \mathcal{N}(0, \mathbf{I})$ is progressively injected following the prescribed noise schedule. The network ϵ_θ is trained to predict the added noise, with the loss defined as:

$$\mathcal{L}(\theta) = \mathbb{E}_{\mathbf{x}_0,k,\boldsymbol{\epsilon}}\left[\left\|\boldsymbol{\epsilon} - \epsilon_\theta(\mathbf{x}_k, k, \mathbf{e}_t, \mathcal{D}_t^{\text{Copula}})\right\|_2^2\right], \boldsymbol{\epsilon} \sim \mathcal{N}(0, \mathbf{I}) \tag{17}$$

Once trained, ϵ_θ guides the reverse diffusion process to generate realistic joint scenarios that reflect both empirical uncertainty and source-load dependencies.

C. Transformer-Based Time-Varying Risk Weighting

The Transformer Layer is designed via an encoder–decoder architecture to generate time-varying risk weights $w_t, t \in [1, T]$ for CVaR risk management as shown in Fig. 3. This layer leverages historical and predicted data through combined self-attention and cross-attention mechanisms.

The encoder processes multivariate historical time-series inputs $\mathbf{X}_{\text{hist}} \in \mathbb{R}^{T_{\text{hist}} \times d_{\text{in}}}$, including PV generation $\mathbf{x}_0^\alpha$, EV charging demand $\mathbf{x}_0^\beta$, source-load dependence $\mathcal{D}_t^{\text{Copula}}$ and weather factors. To capture temporal patterns such as daily cycles, temporal positional encodings $\mathbf{E}_{\text{hist}} \in \mathbb{R}^{T_{\text{hist}} \times d_e}$ are concatenated with the raw input to obtain:

$$\widetilde{\mathbf{X}}_{\text{hist}} = \text{Concat}(\mathbf{X}_{\text{hist}}, \mathbf{E}_{\text{hist}}) \in \mathbb{R}^{T_{\text{hist}} \times (d_{\text{in}} + d_e)}. \tag{18}$$

This representation is projected to the model dimension and passed through a multi-head self-attention layer with L attention heads to analyze the features from different aspects:

$$\text{MultiHead}(\widetilde{\mathbf{X}}_{\text{hist}}) = \text{Concat}(\mathbf{head}_1, ..., \mathbf{head}_L)\mathbf{W}_{\text{hist}}^O \tag{19}$$

$$\mathbf{head}_l = \text{softmax}\left(\frac{\mathbf{Q}_{\text{hist},l}\mathbf{K}_{\text{hist},l}^\top}{\sqrt{d_{\text{in}} + d_e}}\right)\mathbf{V}_{\text{hist},l} \tag{20}$$

with queries $\mathbf{Q}_{\text{hist},l} = \widetilde{\mathbf{X}}_{\text{hist}}\mathbf{W}_{\text{hist},l}^Q$, keys $\mathbf{K}_{\text{hist},l} = \widetilde{\mathbf{X}}_{\text{hist}}\mathbf{W}_{\text{hist},l}^K$, and values $\mathbf{V}_{\text{hist},l} = \widetilde{\mathbf{X}}_{\text{hist}}\mathbf{W}_{\text{hist},l}^V$. Here, $\mathbf{W}_{\text{hist}}^Q, \mathbf{W}_{\text{hist}}^K, \mathbf{W}_{\text{hist}}^V \in \mathbb{R}^{(d_{\text{in}}+d_e)\times d_{\text{model}}}$ and $\mathbf{W}_{\text{hist}}^O \in \mathbb{R}^{(L*d_{\text{model}})\times d_{\text{in}}}$ are the commonly used linear mapping matrices. Then the sequence is processed by a feed-forward network (FFN), dropout, and layer normalization. We denote the intermediate output of the self-attention layer as $\tilde{\mathbf{H}}_{\text{hist}}$, and the final encoder output as $\mathbf{H}_{\text{hist}}$:

$$\tilde{\mathbf{H}}_{\text{hist}} = \text{LayerNorm}\left(\widetilde{\mathbf{X}}_{\text{hist}} + \text{Dropout}(\text{MultiHead}(\widetilde{\mathbf{X}}_{\text{hist}}))\right), \tag{21}$$

$$\mathbf{H}_{\text{hist}} = \text{LayerNorm}\left(\tilde{\mathbf{H}}_{\text{hist}} + \text{Dropout}(\text{FFN}(\tilde{\mathbf{H}}_{\text{hist}}))\right) \tag{22}$$

The decoder receives future features $\mathbf{X}_{\text{pred}} \in \mathbb{R}^{T_{\text{pred}} \times d'_{\text{in}}}$, including statistical descriptors of generated PV and EV scenarios, predicted weather factors, and temporal encodings. After concatenating the position embedding $\mathbf{E}_{\text{pred}} \in \mathbb{R}^{T_{\text{pred}} \times d'_e}$, we obtain $\widetilde{\mathbf{X}}_{\text{pred}} \in \mathbb{R}^{T_{\text{pred}} \times (d'_{\text{in}} + d'_e)}$. The sequence is processed by a multi-head self-attention layer, dropout and layer normalization similar to the encoder structure:

$$\mathbf{H}_{\text{pred}} = \text{LayerNorm}\left(\widetilde{\mathbf{X}}_{\text{pred}} + \text{Dropout}(\text{MultiHead}(\widetilde{\mathbf{X}}_{\text{pred}}))\right) \tag{23}$$

We denote the intermediate output of the cross-attention layer as $\tilde{\mathbf{C}}$, and the final decoder output as $\mathbf{C}$:

$$\tilde{\mathbf{C}} = \text{LayerNorm}\left(\mathbf{H}_{\text{pred}} + \text{Dropout}(\text{CA}(\mathbf{H}_{\text{hist}}, \mathbf{H}_{\text{pred}}))\right), \tag{24}$$

where the cross-attention $\text{CA}(\cdot)$ can be computed as:

$$\text{CA}(\mathbf{H}_{\text{hist}}, \mathbf{H}_{\text{pred}}) = \text{softmax}\left(\frac{\mathbf{H}_{\text{pred}}\mathbf{W}_{\text{pred}}^Q\left(\mathbf{H}_{\text{hist}}\mathbf{W}_{\text{pred}}^K\right)^\top}{\sqrt{d'_{\text{in}} + d'_e}}\right)\mathbf{H}_{\text{hist}}\mathbf{W}_{\text{pred}}^V \tag{25}$$

The sequence is then processed by a feed-forward layer:

$$\mathbf{C} = \text{LayerNorm}\left(\tilde{\mathbf{C}} + \text{Dropout}(\text{FFN}(\tilde{\mathbf{C}}))\right). \tag{26}$$

The representation $\mathbf{C} \in \mathbb{R}^{T \times d_{\text{model}}}$ is passed through a one-dimensional convolution:

$$\mathbf{Z} = \text{Conv1D}(\mathbf{C}) \in \mathbb{R}^{T \times 1}, \tag{27}$$

followed by a softmax normalization:

$$w_t = \frac{\exp(\mathbf{z}_t)}{\sum_{\tau=1}^{T}\exp(\mathbf{z}_\tau)}, \quad t = 1, \ldots, T, \tag{28}$$

where w_t denotes the time-varying risk weight.

To obtain the training targets for the Transformer, we adopt a heuristic search strategy. For each historical day, joint PV-EV scenarios are generated and the CVaR-based optimization formulated in Section II is solved under candidate time-varying risk weights vectors. These candidates are iteratively refined via a guided search process, where the search range at each time step is adaptively adjusted based on scenario volatility to improve efficiency. The weight vector yielding the lowest total cost is selected as the optimal target $\mathbf{w}^*$. The Transformer is then trained in a supervised manner to predict this vector from input features, using the Kullback–Leibler divergence between the predicted and target distributions as the loss function:

$$\mathcal{L}(\theta) = \sum_t w_t^* \log \frac{w_t^*}{w_t(\theta)} \tag{29}$$

This training scheme ensures the model accurately captures temporal risk patterns, enhancing proactive risk management in EVCS optimization in energy market.

IV. Performance Assessment and Numerical Results

The performance of the proposed CDT-RiskNet is evaluated in three aspects: source-load scenario generation, risk-aware stochastic optimization, and adaptability to varying market price conditions. All experiments are implemented in Python 3.8 with the PyTorch package on a laptop equipped with AMD Ryzen 7 5800H CPU and 16 GB RAM. The optimization problems are solved by Gurobi 11.0.0.

A. Data Description and Simulation Setting

The considered cases consist of two EVCS configurations. The small-scale EVCS includes an ESS with 5 battery units, an 80 kW PV installation, 10 V2G-enabled charging piles, and 12 AC piles for inflexible EVs. The scheduling horizon is one day with hourly resolution. The historical data of two sources of uncertainties, PV output and inflexible EV charging demand, comes from real-world data from a PV-ESS-EV integrated charging station located in Guangxi, China. The large-scale EVCS consists of 30 battery units, 400 kW of PV installation, 30 V2G-enabled charging piles, and 20 AC and 10 DC piles for inflexible EVs. The historical PV and EV demand data for the large-scale EVCS are collected from charging facilities in Jiaxing, China. The EV-related parameters, including charging/discharging limits, V2G-enabled EV arrival/departure time distributions, battery efficiency, and cost coefficients, follow the settings in [31]. The weather data for both regions are sourced from [35]. The EV charging data are preprocessed from tabular information into time-series format following the method in [36]. Time-varying purchasing and selling prices for the energy market transactions are adopted from [37].

For the Diffusion module, the number of diffusion steps is set to 50, with the noise schedule parameter configured as 0.008. The hidden layer dimension is set to 128. The model is trained using the Adam optimizer with a learning rate of 1×10^{-4} and a minimum batch size of 32. In the dynamic Copula module, the sliding window length L is set to 24 to effectively capture the temporal dependence in historical data. For the Transformer module, the number of attention heads is set to 4, and d_{model} is set to 128. The model is trained using the Adam optimizer with a learning rate 5×10^{-5} and a minimum batch size of 32.

B. Performance of Source-Load Scenario Generation

To comprehensively evaluate the performance of source–load scenario generation, we conduct experiments on both the small-scale and large-scale EVCS cases and compare the proposed CDT-RiskNet with traditional and recently developed generative models, including GMM, Conditional GAN (CGAN), TimeGAN, and standard Diffusion Models. The evaluation is carried out along two dimensions: generation quality and computational efficiency.

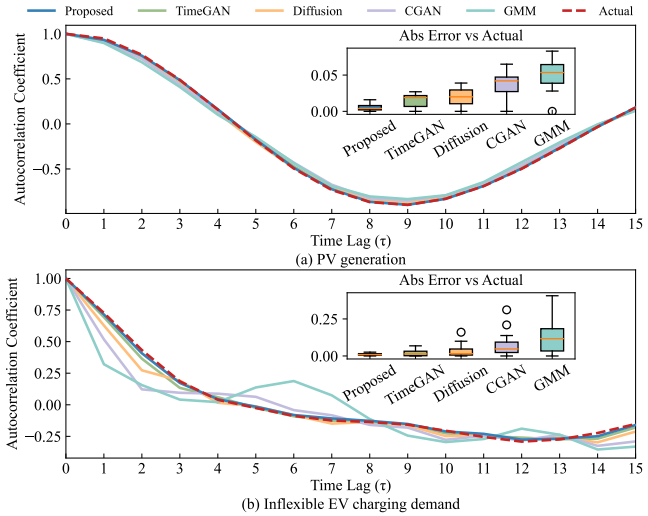

Fig. 4. Autocorrelation coefficients of generated and historical scenarios.

1) Generation quality: Generation quality is assessed in three widely adopted aspects: marginal fidelity, joint fidelity, and scenario diversity, which collectively characterize the accuracy and richness of the generated PV–EV scenarios.

Marginal fidelity: Marginal fidelity quantifies the preservation of each variable's statistics, assessed by Temporal Consistency (TC) and Statistical Consistency (SC) [38].

TC evaluates whether the generated time series preserves the temporal dependence structure of historical data. The autocorrelation coefficient $R(\tau)$ is commonly used to evaluate TC, defined at lag τ as:

$$R(\tau) = \frac{\mathbb{E}\left[(S_t - \mu)(S_{t+\tau} - \mu)\right]}{\sigma^2} \tag{30}$$

where S_t represents a time sequence of generated or historical scenarios with mean μ and variance σ^2.

Fig. 4 shows that the proposed method closely aligns with real data, particularly for inflexible EV demand, for which traditional models deviate significantly. Box plots of absolute autocorrelation errors further confirm that CDT-RiskNet better captures intrinsic temporal patterns than baseline methods.

SC measures how well the marginal statistical distributions of the generated scenarios match those of the historical data. SC is evaluated via empirical cumulative distribution functions (ECDF) in Fig. 5. The actual single-day scenario yields a stepwise ECDF, while generated scenario with M samples forms smoother curves. GMM captures the strict zero values, matching the actual ECDF around zero, but fails on high-value fluctuations. Deep generative models better fit nonlinear dynamics but struggle near zero, due to reliance on continuous latent representations. Mean absolute error (MAE) of ECDF shown in the inset radar charts indicates that the proposed method achieves better statistical consistency than baselines.

Joint fidelity: Joint fidelity measures how well the generated PV-EV scenarios preserve their joint structure. The Energy Score (ES) assesses overall distributional similarity, and the Variogram Score (VS) captures temporal dependencies, with lower values indicating better fidelity [39]. Their joint

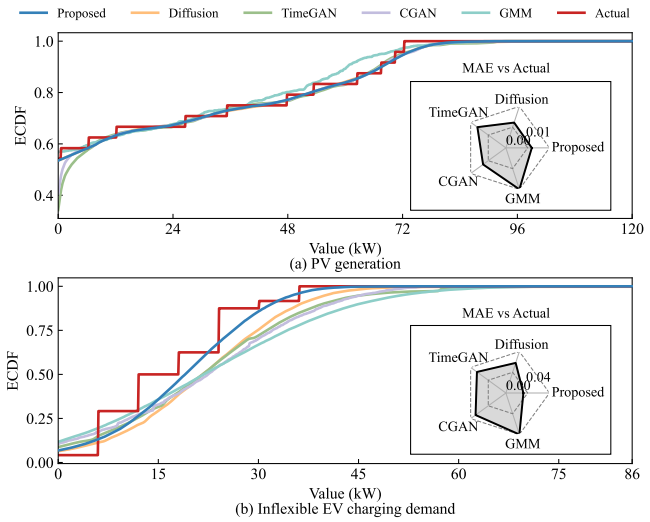

Fig. 5. ECDFs of generated and actual scenarios.

TABLE II
PERFORMANCE COMPARISON USING ES AND VS

Method	ES (PV)	ES (EV)	Joint ES	VS (PV)	VS (EV)	Joint VS
Proposed	**0.059**	**0.368**	**0.377**	**0.551**	**20.608**	**25.025**
TimeGAN	0.071	0.392	0.404	0.679	22.113	28.126
Diffusion	0.063	0.385	0.430	0.642	21.875	27.778
CGAN	0.085	0.410	0.472	0.813	25.400	33.589
GMM	0.113	0.468	0.521	1.129	37.025	45.956

extensions, Joint ES and Joint VS, apply these principles to the combined PV-EV scenario space to assess joint fidelity. Formally, they are defined as:

$$\mathrm{ES} = \frac{1}{M}\sum_{m=1}^{M}\left\|\mathbf{x}_0^{(m)} - \mathbf{x}_0\right\| - \frac{1}{2M^2}\sum_{n,m=1}^{M}\left\|\mathbf{x}_0^{(m)} - \mathbf{x}_0^{(n)}\right\| \tag{31}$$

$$\mathrm{VS} = \sum_{i,j=t+1}^{t+T}\left(|x_{0,i} - x_{0,j}|^{\frac{1}{2}} - \frac{1}{M}\sum_{m=1}^{M}\left|x_{0,i}^{(m)} - x_{0,j}^{(m)}\right|^{\frac{1}{2}}\right)^2 \tag{32}$$

For each method, ES and VS are computed for PV and EV, and for their concatenated PV-EV vectors. The joint metrics assess the model's ability to preserve cross-variable dependence, while the marginal scores reflect marginal fidelity. As shown in Table II, the proposed method achieves the lowest joint ES and VS. Diffusion performs similarly in marginal scores but worse joint scores, due to lack of explicit dependence modeling.

Diversity: Diversity, defined as the spread and richness of generated scenarios, is evaluated by the Discriminator Score (DS) [16], which quantifies the difficulty for a binary classifier to distinguish generated profiles from real ones. Limited diversity yields lower loss, as the classifier easily identifies synthetic data, while high diversity makes classification harder, increasing loss. The ideal DS is $\ln(2) \approx 0.693$, achieved when real and generated samples are indistinguishable.

Fig. 6 shows that the proposed CDT-RiskNet consistently attains higher DS values for all categories, approaching the ideal value $\ln(2)$, with narrower confidence intervals. Compared to

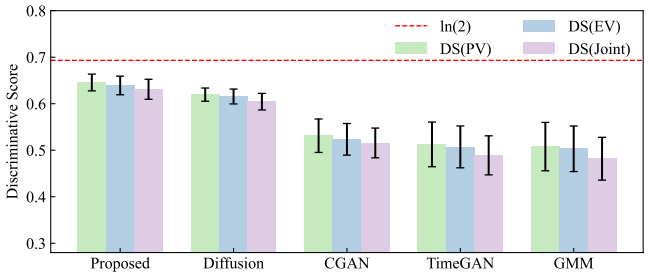

Fig. 6. Discriminative scores of different generation methods.

TABLE III
SCENARIO GENERATION PERFORMANCE ON THE LARGE-SCALE EVCS

Method	TC MAE ↓		SC MAE ↓		Joint ES ↓	Joint VS ↓	Joint DS ↑
	PV	EV	PV	EV			
Proposed	0.0068	0.0149	0.0137	0.0418	0.392	26.84	0.618
TimeGAN	0.0186	0.0247	0.0178	0.0819	0.421	30.12	0.472
Diffusion	0.0229	0.0409	0.0146	0.0713	0.448	29.58	0.586
CGAN	0.0415	0.0856	0.0139	0.0837	0.493	35.74	0.498
GMM	0.0562	0.1428	0.0213	0.0974	0.543	48.61	0.463

TABLE IV
TRAINING AND INFERENCE TIME FOR SCENARIO GENERATION

Method	Training Time (min)		Inference Time (s)	
	Small	Large	Small	Large
Proposed	52.45	57.98	284.25	286.80
TimeGAN	19.45	18.71	12.82	13.00
Diffusion	47.82	48.39	271.92	270.36
CGAN	11.66	11.24	6.49	6.22
GMM	0.05	0.05	0.82	0.83

baselines, it demonstrates superior diversity and realism, which is critical for effective stochastic optimization and robust risk management in EV charging operations.

Finally, for the large-scale EVCS, summary metrics are computed for each method, including MAE of autocorrelation coefficient for TC, MAE of ECDF for SC, joint ES/VS and the DS. The results are reported in Table III to examine whether the above conclusions generalize across different EVCS configurations. It is observed that CDT-RiskNet achieves the lowest MAE for TC and SC, the smallest joint ES and VS, and the highest DS among all baselines on the large-scale EVCS, indicating that the proposed method generalizes well to different EVCS configurations.

2) Computational efficiency: Computational efficiency is evaluated through the training time and the inference time of each method on both EVCSs, as summarized in Table IV.

Comparing across methods, GMM achieves the shortest training and inference times due to its simple parametric structure. CGAN and TimeGAN are also computationally efficient, as both generate samples through a single forward pass without iterative refinement. In contrast, Diffusion and the proposed CDT-RiskNet require multi-step denoising, leading to higher computational costs. CDT-RiskNet incurs slightly longer runtime than the standard Diffusion model because the dynamic Copula module introduces an extra preprocessing step and an additional input dimension. Given the improvements in marginal fidelity, joint fidelity, and diversity, this moderate overhead is acceptable for day-ahead scenario generation.

TABLE V
EXPERIMENTAL CONFIGURATIONS

Strategy	Scenario Generation	Risk Weighting Strategy
Baseline1 (B1)	GMM	Static ($w_t = 1/T$)
Baseline2 (B2)	TimeGAN	Static ($w_t = 1/T$)
Baseline3 (B3)	Proposed	Static ($w_t = 1/T$)
Baseline4 (B4)	Proposed	Empirical TW-CVaR
Baseline5 (B5)	Proposed	LSTM-based TW-CVaR
Baseline6 (B6)	Proposed	Transformer (Variance-label)
Baseline7 (B7)	Proposed	E2E-Transformer (CVaR-loss)
Proposed (P1)	Proposed	Proposed

Moreover, training is performed offline, and the inference times of 284.25 s and 286.80 s remain well within the requirements of day-ahead operation, where scenario generation only needs to be completed once per scheduling cycle.

Comparing across EVCS scales, the training and inference times are nearly identical for the small and large stations. The computational complexity of generative models is determined by the sequence length and network architecture rather than by the magnitude of the charging power. As a result, applying the models to a larger station does not increase the runtime. This demonstrates that CDT-RiskNet is scalable in terms of computational efficiency.

C. Performance of Risk Weight Generation and EVCS Stochastic Operation

To evaluate CDT-RiskNet in EVCS decision-making, the performance of both risk weight generation and downstream operation is compared across the strategies summarized in Table V. Strategies B1–B3 employ static equal weights with different scenario generation methods. Strategies B4–B7 all adopt the TW-CVaR formulation but differ in how the time-varying weights w_t are obtained. B4 uses empirical volatility-based weights, and B5 forecasts w_t via an LSTM model. B6 trains a Transformer on variance-based labels derived from scenario dispersion, whereas B7 also employs Transformer but learns w_t end-to-end by minimizing a differentiable surrogate CVaR-loss. P1 adopts the proposed CDT-RiskNet framework.

To validate the robustness across different uncertainty levels, two representative cases of the small-scale EVCS are considered: **(i) a sunny-day case** with high PV availability and moderate EV load, and **(ii) a rainy-day case** with suppressed PV output and higher EV load. These cases together demonstrate the generalization capability of the proposed CDT-RiskNet. All experiments are also conducted on the large-scale EVCS.

1) Risk weight generation: For the sunny-day case, Fig. 7 shows that the generated scenarios can cover the actual ones, while wider bands and mean shifts in certain periods imply higher risks. The high-risk hours are highlighted in red and medium-risk hours in yellow. The weight pattern aligns with scenario uncertainty, reflecting the method's ability to capture temporal variations. Fig. 8 compares the normalized hourly risk weights generated by six strategies: B3, B4, B5, B6, B7, and P1. The risk weights for each strategy are independently normalized over 24 hours. The medium-risk and high-risk periods are defined as weights exceeding 0.5 and 0.8, respectively. B3 applies static weights, ignoring temporal variability.

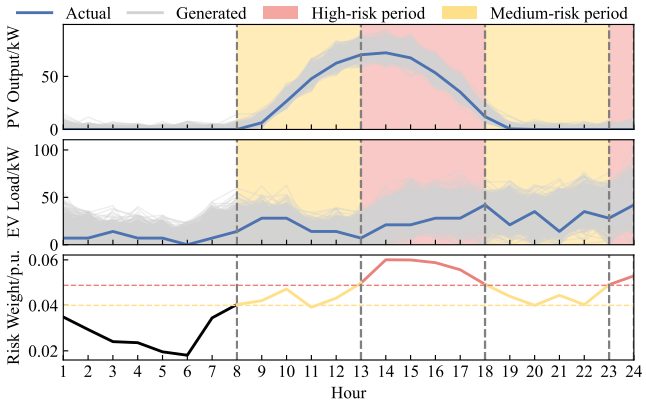

Fig. 7. Illustration of scenario distributions and learned risk weights under P1 in the sunny-day case.

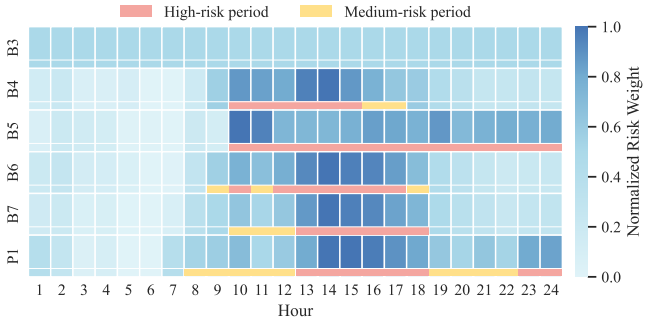

Fig. 8. Comparison of hourly risk weights generated by different strategies in the sunny-day case.

B4 captures midday risk based on historical patterns but lacks scenario sensitivity. B5 partially identifies afternoon and evening as relatively higher risk, but is limited by weak long-range modeling. For B6, dispersion does not fully represent tail-risk characteristics, leading to less accurate identification of high-risk hours. B7 improves by training with a surrogate CVaR-loss objective, which provides a more targeted emphasis on adverse outcomes; however, the surrogate loss still exhibits deviations. In contrast, P1 generates a more refined risk allocation, effectively capturing temporal risk dynamics.

For the rainy-day case, Fig. 9 also shows good alignment with the observed fluctuations and deviations. These results confirm the generalization capability of the proposed method across different uncertainty profiles. Fig. 10 shows the normalized hourly risk weights in rainy-day case. P1 more accurately integrates historical volatility and future scenario statistics to generate time-varying risk weights, effectively capturing the evolving uncertainty patterns.

To quantitatively assess the accuracy of the learned weights, a reference hindsight-optimal profile w_t^* is constructed offline by repeatedly solving the TW-CVaR-based optimization model under candidate weight vectors. The vector that yields the minimum operational cost is selected as w_t^*. Using w_t^* as the benchmark, we compute the mean absolute percentage error (MAPE) of the generated weights, as summarized in Table VI. Across all cases, P1 achieves the lowest MAPE, demonstrating

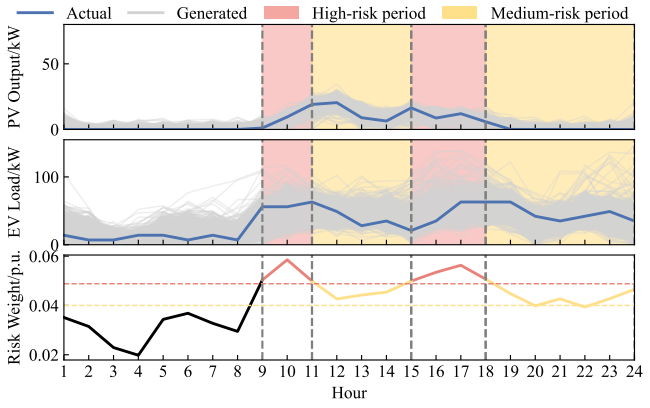

Fig. 9. Illustration of scenario distributions and learned risk weights under P1 in the rainy-day case.

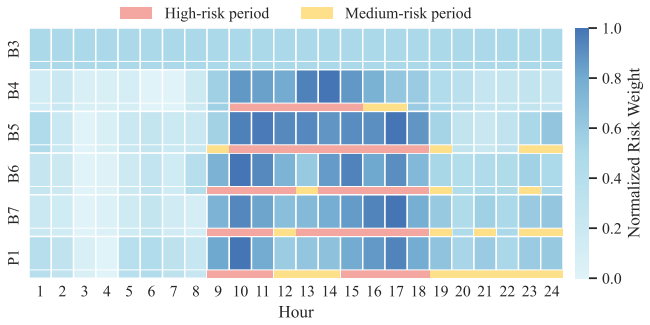

Fig. 10. Comparison of hourly risk weights generated by different strategies in the rainy-day case.

TABLE VI
MAPE OF GENERATED RISK WEIGHTS RELATIVE TO HINDSIGHT-OPTIMAL PROFILE

Strategy	Small–Scale (Sunny)	Small–Scale (Rainy)	Large-Scale
B4	40.84%	41.44%	34.72%
B5	21.41%	16.48%	18.36%
B6	14.26%	6.96%	11.04%
B7	10.79%	5.70%	8.27%
P1	**4.63%**	**3.59%**	**5.41%**

its superior ability to approximate the optimal risk profile.

In terms of computational efficiency, the risk-weighting module introduces negligible additional cost compared with scenario generation and stochastic optimization. All training procedures are conducted offline, and the trained Transformer requires only millisecond-level inference during deployment. Therefore, the proposed dynamic risk–weighting mechanism does not impose any practical computational burden.

2) Stochastic optimization performance analysis: Fig. 11 illustrates the chronological operational decisions under strategies P1, B7, and B4 in the small-scale EVCS for the sunny-day case. The figure reports the aggregated charging and discharging behaviors of V2G-enabled EVs and ESS, and the buying and selling decisions in the energy market (EM). For reference, the mean profiles of PV generation and inflexible EV charging demand across scenarios are also overlaid.

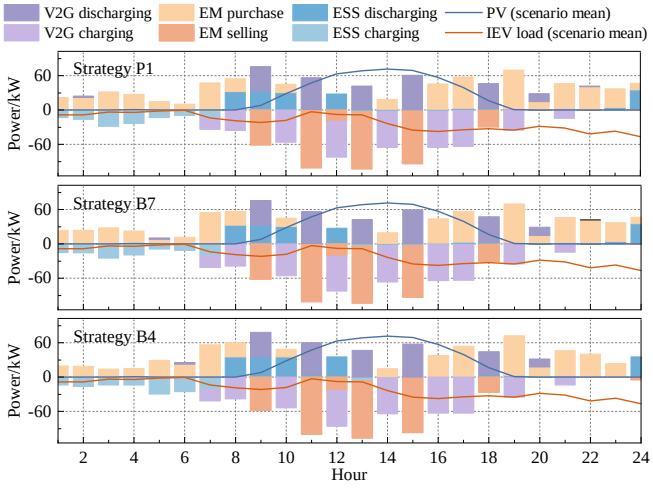

Fig. 11. Chronological operational decisions of the small-scale EVCS under different strategies in the sunny-day case.

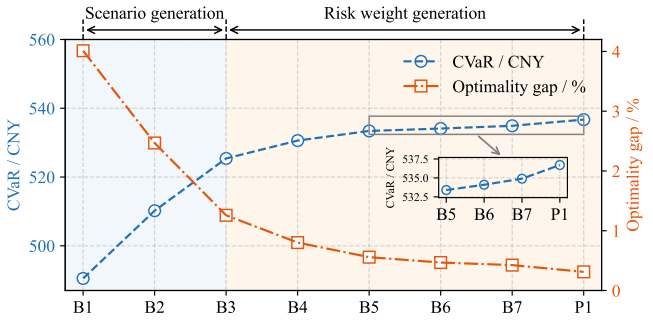

Fig. 12. Comparison of CVaR and optimality gap across different strategies in sunny-day case.

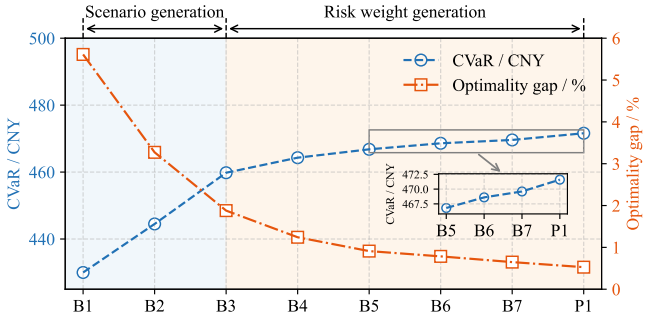

Fig. 13. Comparison of CVaR and optimality gap across different strategies in rainy-day case.

To assess CDT-RiskNet in risk-aware EVCS scheduling, CVaR of the profit distribution and optimality gap are compared. The scenario set and time-varying risk weights serve as inputs to the stochastic optimization model. The optimality gap is defined relative to a hindsight-optimal benchmark with perfect foresight of PV and EV profiles. For sunny-day case, Fig. 12 shows that improving scenario generation method from B1 to B3 significantly reduces the gap and raises CVaR, indicating that more accurate uncertainty description yields more profitable and robust decisions. Further improvements

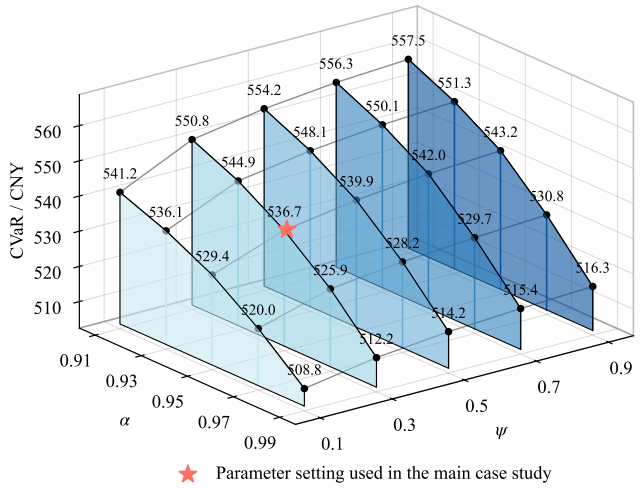

Fig. 14. Sensitivity of profit-based CVaR to the confidence level α and risk-aversion coefficient ψ under P1.

TABLE VII
SUMMARY OF STOCHASTIC OPTIMIZATION PERFORMANCE UNDER P1

Case	CVaR (CNY)	Optimality Gap (%)	Optimization Time (s)
Small–scale (Sunny)	536.7	0.312	16.42
Small–scale (Rainy)	471.6	0.527	14.31
Large-scale	1512.4	0.224	62.62

from B3 to B7, and finally to P1, consistently enhance both metrics, with P1 achieving the smallest gap of 0.312% and the highest CVaR of 536.7 CNY. This demonstrates the benefit of time-varying risk allocation. The results indicate that scenario quality is the dominant contributor, while adaptive weighting provides additional gains. For rainy-day case, Fig. 13 shows that P1 gets the highest CVaR of 471.6 CNY and the smallest optimality gap of 0.527%. These results confirm the generalization of CDT-RiskNet across conditions.

To further examine the influence of the risk parameters, Fig. 14 reports profit-based CVaR under different confidence levels α and risk-aversion coefficients ψ. The results show that CVaR decreases nonlinearly with increasing α, reflecting stricter tail-profit evaluation, while it increases with ψ with diminishing marginal gains. The parameter setting adopted in the main case study lies in the middle of this surface, balancing conservativeness and profitability.

As shown in Table VII, optimization time increases with EVCS scale due to higher-dimensional decision variables and additional constraints introduced by more V2G piles and battery units. The KKT-based reformulation of the lower-level problem further enlarges the complementarity structure, leading to increased computation time. This explains the rise from roughly 15-16 s in the small-scale cases to 62.62 s in the large-scale EVCS. Nevertheless, all solve times remain well within the acceptable range for day-ahead market operation.

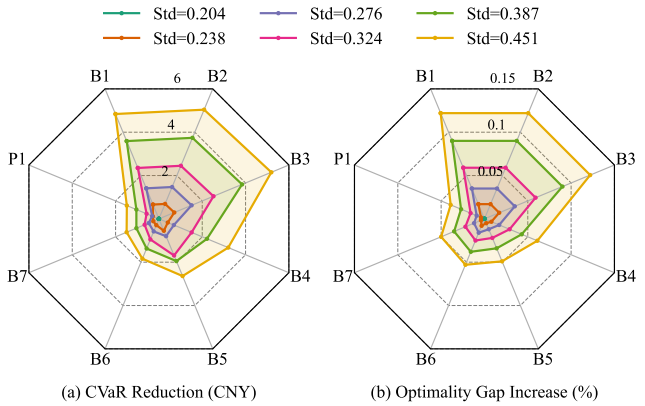

Fig. 15. Comparative analysis of strategy performance under varying electricity price volatility: (a) CVaR reduction and (b) optimality gap increase, both relative to the reference case (Std = 0.204).

TABLE VIII
PERFORMANCE OF P1 ON THE LARGE-SCALE EVCS UNDER VARYING ELECTRICITY PRICE VOLATILITY

Price Std	CVaR Reduction (CNY)	Optimality Gap Increase (%)
0.204 (reference)	/	/
0.238	1.6	0.021
0.276	3.4	0.037
0.324	6.1	0.063
0.387	9.8	0.089
0.451	13.5	0.124

D. Energy Market Adaptability under Price Volatility

To evaluate the adaptability of CDT-RiskNet under varying market conditions, a series of case studies is conducted with increasing electricity price volatility while keeping the overall arbitrage space constant. With PV and EV scenarios held fixed, the observed performance differences mainly reflect each method's ability to perceive and adapt to price volatility.

Fig. 15 illustrates the variations in CVaR and optimality gap across different electricity price standard deviations (Std), relative to the baseline case with Std $= 0.204$. P1 exhibits a minimal CVaR reduction and optimality gap increase, demonstrating its superior capability to perceive and mitigate time-varying price risks. Table VIII reports the metrics for P1 on the large-scale EVCS under increasing electricity price volatility. These results suggest that as electricity markets become more volatile, the operational risk faced by EVCS operators intensifies, amplifying the need for flexible and temporally adaptive risk management mechanisms. CDT-RiskNet offers a unified solution to address this challenge.

V. CONCLUSION

This paper proposes CDT-RiskNet, a Copula-Diffusion-Transformer framework for risk-aware stochastic optimization of EV charging stations in energy markets. The proposed model addresses two major challenges in such decision-making: the generation of realistic source-load joint scenarios and the dynamic quantification of risk across time. By integrating copula-based scenario generation with Transformer-driven

dynamic risk weighting under a CVaR formulation, the model jointly captures PV–EV dependencies and time-varying risk.

Comprehensive case studies with real-world data from EVCSs of different scales show that CDT-RiskNet improves scenario fidelity, enhances risk-aware decision-making, and adapts to market volatility, thereby strengthening the effectiveness and robustness of EVCS operations under uncertainty. Future work will extend the framework to multi-agent markets and incorporate more detailed battery degradation models.

REFERENCES

[1] D. Matkovic, T. M. Pilski, and T. Capuder, "Participation of electric vehicle charging station aggregators in the day-ahead energy market using demand forecasting and uncertainty-based pricing," *Energy*, p. 136299, 2025.

[2] International Energy Agency (IEA), "Global ev outlook 2025," Paris, 2025, licence: CC BY 4.0. [Online]. Available: https://www.iea.org/reports/global-ev-outlook-2025

[3] L. Affolabi, M. Shahidehpour, W. Gan, M. Yan, B. Chen, S. Pandey, A. Vukojevic, E. A. Paaso, A. Alabdulwahab, and A. Abusorrah, "Optimal transactive energy trading of electric vehicle charging stations with on-site pv generation in constrained power distribution networks," *IEEE Transactions on Smart Grid*, vol. 13, no. 2, pp. 1427–1440, 2021.

[4] Y. Jiang, T. Ortmeyer, and M. Fan, "Data-driven fast uncertainty assessment of distribution systems with correlated ev charging demand and renewable generation," *IEEE Transactions on Sustainable Energy*, vol. 14, no. 3, pp. 1446–1456, 2023.

[5] Q. Wang, X. Zhang, and D. Xu, "Battery energy storage system planning based on super-resolution source-load uncertainty reconstruction," *IEEE Transactions on Smart Grid*, vol. 15, no. 1, pp. 581–594, 2023.

[6] J. C. Do Prado and U. Chikezie, "A decision model for an electricity retailer with energy storage and virtual bidding under daily and hourly cvar assessment," *IEEE access*, vol. 9, pp. 106 181–106 191, 2021.

[7] M. Kim, T. Park, J. Jeong, and H. Kim, "Stochastic optimization of home energy management system using clustered quantile scenario reduction," *Applied Energy*, vol. 349, p. 121555, 2023.

[8] A. Dolatabadi, B. Mohammadi-Ivatloo, M. Abapour, and S. Tohidi, "Optimal stochastic design of wind integrated energy hub," *IEEE Transactions on Industrial Informatics*, vol. 13, no. 5, pp. 2379–2388, 2017.

[9] Z. Wang, C. Shen, and F. Liu, "A conditional model of wind power forecast errors and its application in scenario generation," *Applied energy*, vol. 212, pp. 771–785, 2018.

[10] R. Carmona and X. Yang, "Joint granular model for load, solar and wind power scenario generation," *IEEE Transactions on Sustainable Energy*, vol. 15, no. 1, pp. 674–686, 2023.

[11] A. Bagheri, J. Wang, and C. Zhao, "Data-driven stochastic transmission expansion planning," *IEEE Transactions on Power Systems*, vol. 32, no. 5, pp. 3461–3470, 2016.

[12] Z. Li, X. Peng, W. Cui, Y. Xu, J. Liu, H. Yuan, C. S. Lai, and L. L. Lai, "A novel scenario generation method of renewable energy using improved vaegan with controllable interpretable features," *Applied Energy*, vol. 363, p. 122905, 2024.

[13] H. Wang, B. Qin, S. Hong, X. Xu, Y. Su, T. Lu, and T. Ding, "Enhanced gan based joint wind-solar-load scenario generation with extreme weather labelling," *IEEE Transactions on Smart Grid*, 2025.

[14] Q. Wang, X. Zhang, and D. Xu, "Source-load scenario generation based on weakly supervised adversarial learning and its data-driven application in energy storage capacity sizing," *IEEE Transactions on Sustainable Energy*, vol. 14, no. 4, pp. 1918–1932, 2023.

[15] X. Dong, Z. Mao, Y. Sun, and X. Xu, "Short-term wind power scenario generation based on conditional latent diffusion models," *IEEE Transactions on Sustainable Energy*, vol. 15, no. 2, pp. 1074–1085, 2023.

[16] S. Li, H. Xiong, and Y. Chen, "Diffcharge: Generating ev charging scenarios via a denoising diffusion model," *IEEE Transactions on Smart Grid*, vol. 15, no. 4, pp. 3936–3949, 2024.

[17] Z. Wang and H. Zhang, "Customized load profiles synthesis for electricity customers based on conditional diffusion models," *IEEE Transactions on Smart Grid*, 2024.

[18] S. Feng, C. Miao, Z. Zhang, and P. Zhao, "Latent diffusion transformer for probabilistic time series forecasting," in *Proceedings of the AAAI Conference on Artificial Intelligence*, vol. 38, no. 11, 2024, pp. 11 979–11 987.

[19] W. Zhao, Z. Shao, S. Yang, and X. Lu, "A novel conditional diffusion model for joint source-load scenario generation considering both diversity and controllability," *Applied Energy*, vol. 377, p. 124555, 2025.

[20] J. Fairbrother, A. Turner, and S. W. Wallace, "Problem-driven scenario generation: an analytical approach for stochastic programs with tail risk measure," *Mathematical Programming*, vol. 191, no. 1, pp. 141–182, 2022.

[21] M. Asensio and J. Contreras, "Stochastic unit commitment in isolated systems with renewable penetration under cvar assessment," *IEEE Transactions on Smart Grid*, vol. 7, no. 3, pp. 1356–1367, 2015.

[22] Y. Zou, Y. Xu, and C. Zhang, "A risk-averse adaptive stochastic optimization method for transactive energy management of a multi-energy microgrid," *IEEE Transactions on Sustainable Energy*, vol. 14, no. 3, pp. 1599–1611, 2023.

[23] D. Xiao, H. Chen, W. Cai, C. Wei, and Z. Zhao, "Integrated risk measurement and control for stochastic energy trading of a wind storage system in electricity markets," *Protection and Control of Modern Power Systems*, vol. 8, no. 4, pp. 1–11, 2023.

[24] M. Daneshvar, B. Mohammadi-Ivatloo, and K. Zare, "A fair risk-averse stochastic transactive energy model for 100% renewable multi-microgrids in the modern power and gas incorporated network," *IEEE Transactions on Smart Grid*, vol. 14, no. 3, pp. 1933–1945, 2022.

[25] W. Qin, X. Li, X. Jing, Z. Zhu, R. Lu, and X. Han, "Multi-temporal optimization of virtual power plant in energy-frequency regulation market under uncertainties," *Journal of Modern Power Systems and Clean Energy*, 2024.

[26] M. Wang, X. Li, C. Dong, Y. Mu, H. Jia, and F. Li, "Day-ahead optimal bidding for a retailer with flexible participation of electric vehicles," *IEEE Transactions on Smart Grid*, vol. 14, no. 2, pp. 1482–1494, 2022.

[27] Y. Vardanyan and M. R. Hesamzadeh, "The coordinated bidding of a hydropower producer in three-settlement markets with time-dependent risk measure," *Electric Power Systems Research*, vol. 151, pp. 40–58, 2017.

[28] J. Wang, N. Xie, C. Huang, and Y. Wang, "Two-stage stochastic-robust model for the self-scheduling problem of an aggregator participating in energy and reserve markets," *Protection and control of modern power systems*, vol. 8, no. 3, pp. 1–20, 2023.

[29] J. Yang, H. He, X. Zhao, J. Wang, T. Yao, H. Cao, and M. Wan, "Day-ahead pv power forecasting model based on fine-grained temporal attention and cloud-coverage spatial attention," *IEEE Transactions on Sustainable Energy*, vol. 15, no. 2, pp. 1062–1073, 2023.

[30] Y. Zhou, D. K. Yau, P. You, and P. Cheng, "Optimal-cost scheduling of electrical vehicle charging under uncertainty," *IEEE Transactions on Smart Grid*, vol. 9, no. 5, pp. 4547–4554, 2017.

[31] J. Wang, Z. Wang, B. Yang, F. Liu, W. Wei, and X. Guan, "V2g for frequency regulation service: a stackelberg game approach considering endogenous uncertainties," *IEEE Transactions on Transportation Electrification*, 2024.

[32] L. Wang, J. Kwon, N. Schulz, and Z. Zhou, "Evaluation of aggregated ev flexibility with tso-dso coordination," *IEEE Transactions on Sustainable Energy*, vol. 13, no. 4, pp. 2304–2315, 2022.

[33] A. Najafi-Ghalelou, M. Khorasany, and R. Razzaghi, "Stochastic two-stage coordination of electric vehicles in distribution networks: a multi-follower bi-level approach," *Journal of Cleaner Production*, vol. 414, p. 137610, 2023.

[34] X. Zhang, Y. Zhou, S. Ge, H. Liu, and B. Yang, "Data-driven stochastic planning for network constrained energy sharing in microgrids," in *2024 IEEE Power & Energy Society General Meeting (PESGM)*. IEEE, 2024, pp. 1–5.

[35] Huiju environmental. [EB/OL]. [Online]. Available: http://www.hjhj-e.com/

[36] Z. N. Bampos, V. M. Laitsos, K. D. Afentoulis, S. I. Vagropoulos, and P. N. Biskas, "Electric vehicles load forecasting for day-ahead market participation using machine and deep learning methods," *Applied Energy*, vol. 360, p. 122801, 2024.

[37] J. Han, Y. Fang, E. Du, P. Yong, N. Zhang, and N. Liu, "Eliminating distribution network congestion based on spatial-temporal migration of multiple base stations," *IEEE Transactions on Smart Grid*, 2024.

[38] Y. Wang, Y. Liu, and Q. Yang, "Operational scenario generation and forecasting for integrated energy systems," *IEEE Transactions on Industrial Informatics*, vol. 20, no. 2, pp. 2920–2931, 2023.

[39] M. Scheuerer and T. M. Hamill, "Variogram-based proper scoring rules for probabilistic forecasts of multivariate quantities," *Monthly Weather Review*, vol. 143, no. 4, pp. 1321–1334, 2015.